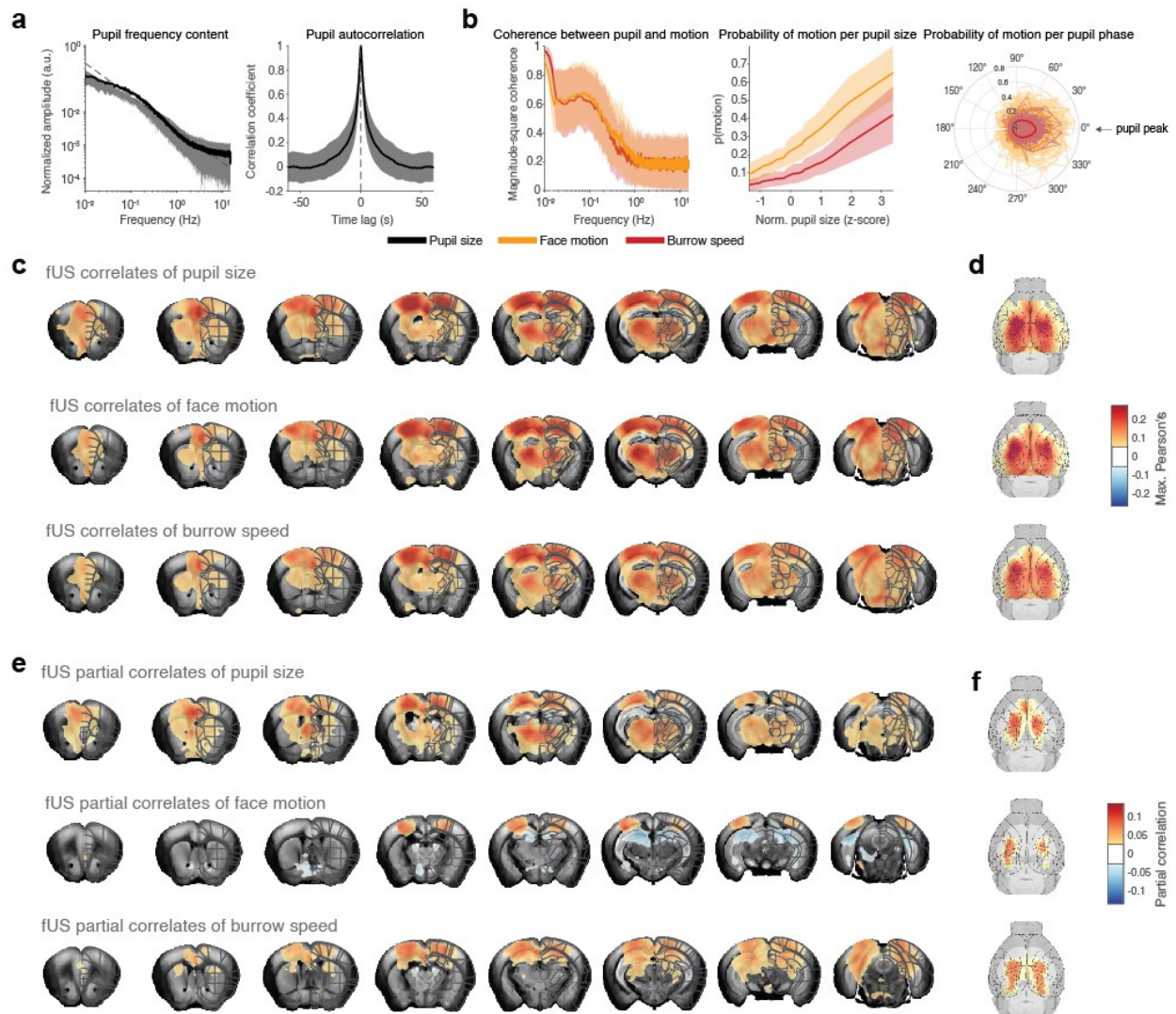
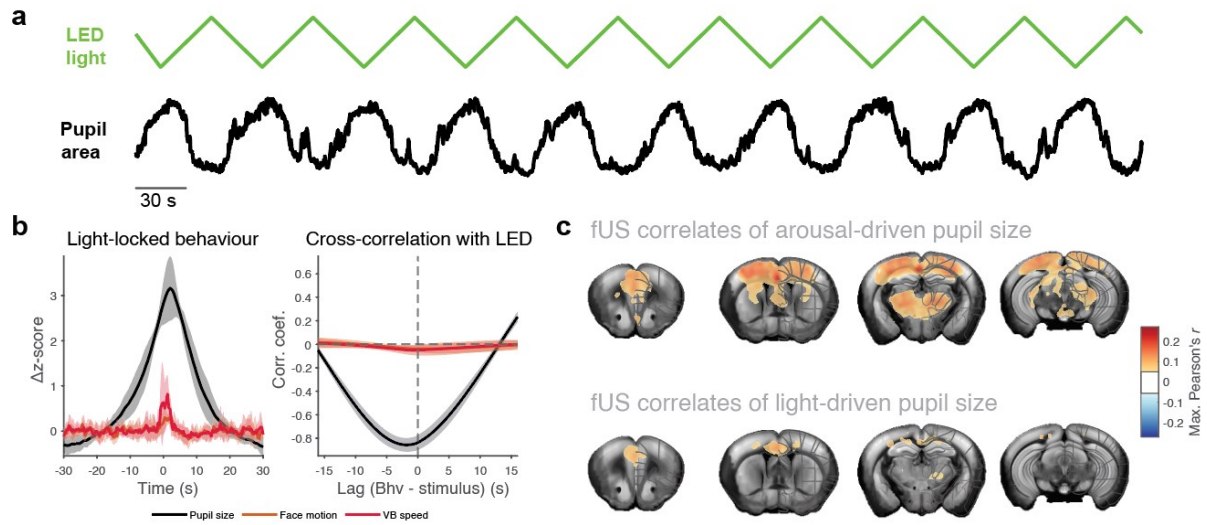


Supplementary figures



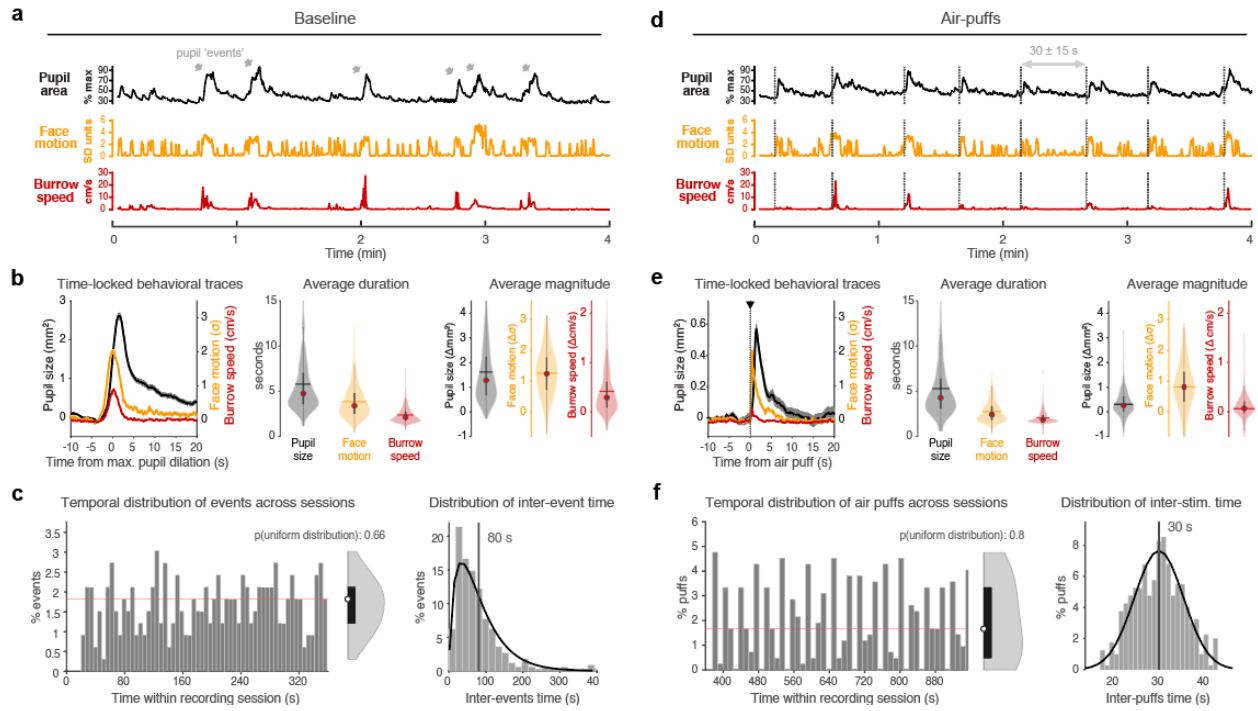
Supp. Figure 1. Pupil and motion reflect the same underlying spontaneous arousal fluctuations, but pupil is more explanatory of brain-wide fUS signal.

a. Left: pupil frequency content. Right: pupil autocorrelation. **b.** Left: coherence between pupil and burrow and face motion. Center: probability of motion as a function of normalized pupil size. Right: probability of motion as a function of pupil phase. **c.** Brain-wide maximum correlation map of pupil size (*top*), face motion (*middle*) and virtual burrow speed (*bottom*). **d.** Cortical views of the maps in **c**. **e.** As **c**., but for brain-wide partial correlation maps. **f.** Cortical views of the maps in **e**.



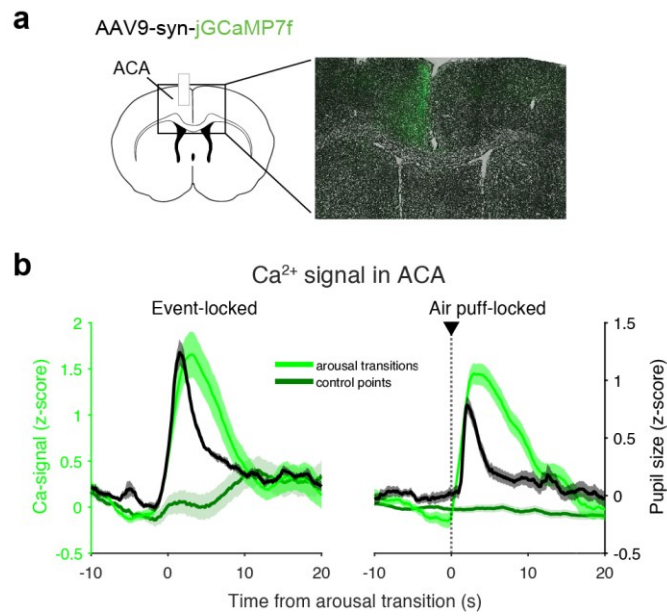
Supp. Figure 2. Pupillary change alone does not evoke the arousal pattern.

a. Ramping light stimulus used to trigger the photopupillary reflex (*top*) and representative associated pupil size trace (*bottom*). **b.** Average behavioral metrics locked to the timepoint of maximum illumination (*left*) and cross-correlation between the light stimulus and the behavioral traces (*right*). **c.** Brain-wide 0-lag correlation map of pupil size during constant illumination (*top*) and during ramping light stimulation (*bottom*) with fUS signal, with fine brain regions overlaid



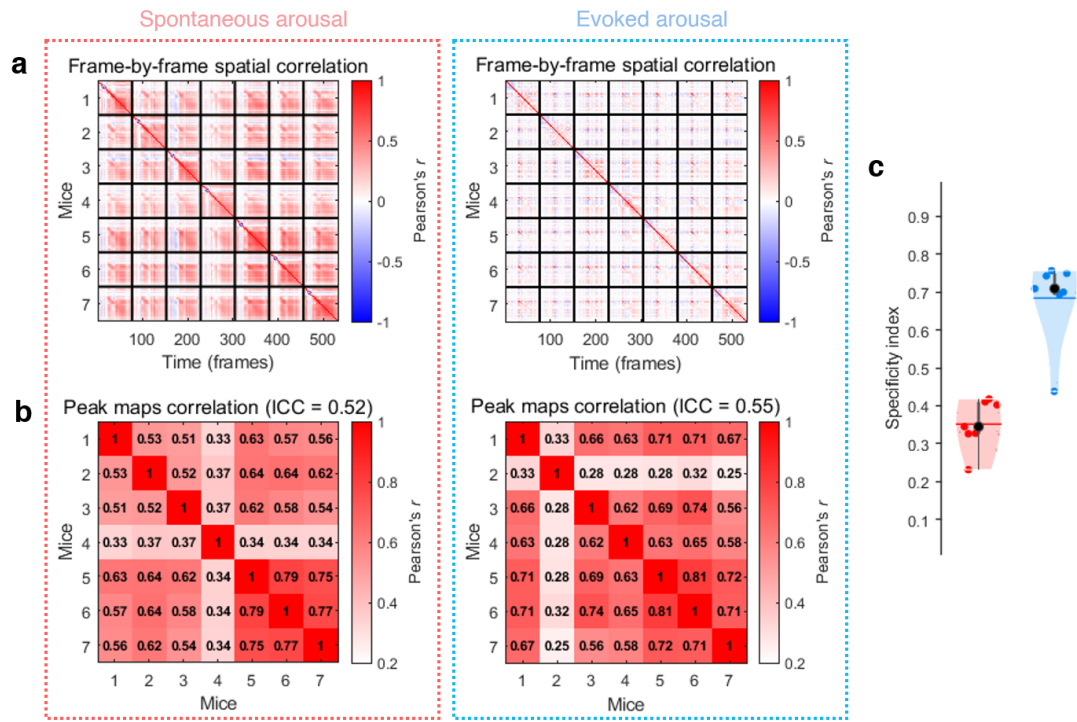
Supp. Figure 3. Identification and behavioral characterization of spontaneous and evoked arousal transitions.

a. Example time series of behavioral metrics during a stimulus-free recording, with spontaneous arousal events highlighted. **b.** Left: average time-locked behavioral metrics during spontaneous arousal transitions. Center: distribution of each behavioral metric bout duration (full-width at half-maximum) across mice. Right: distribution of each behavioral metric peak value across mice. **c.** Left: probability of spontaneous pupil events throughout the typical recording session length. Center: probability distribution for the spontaneous events occurrence, including the probability of this distribution being uniform (calculated via Kolmogorov-Smirnov test). Right: histogram of the inter-event times, with average time highlighted. **d.** Example time series of behavioral metrics during an air puff recording, with the air puffs highlighted. **e.** As in **b**, but for stimulus-locked behavioral metrics during evoked arousal transitions. **f.** As in **c**, but for the probability of pseudorandomized air puffs throughout the typical recording session length (*left, center*) and for inter-stimulus times (*right*).



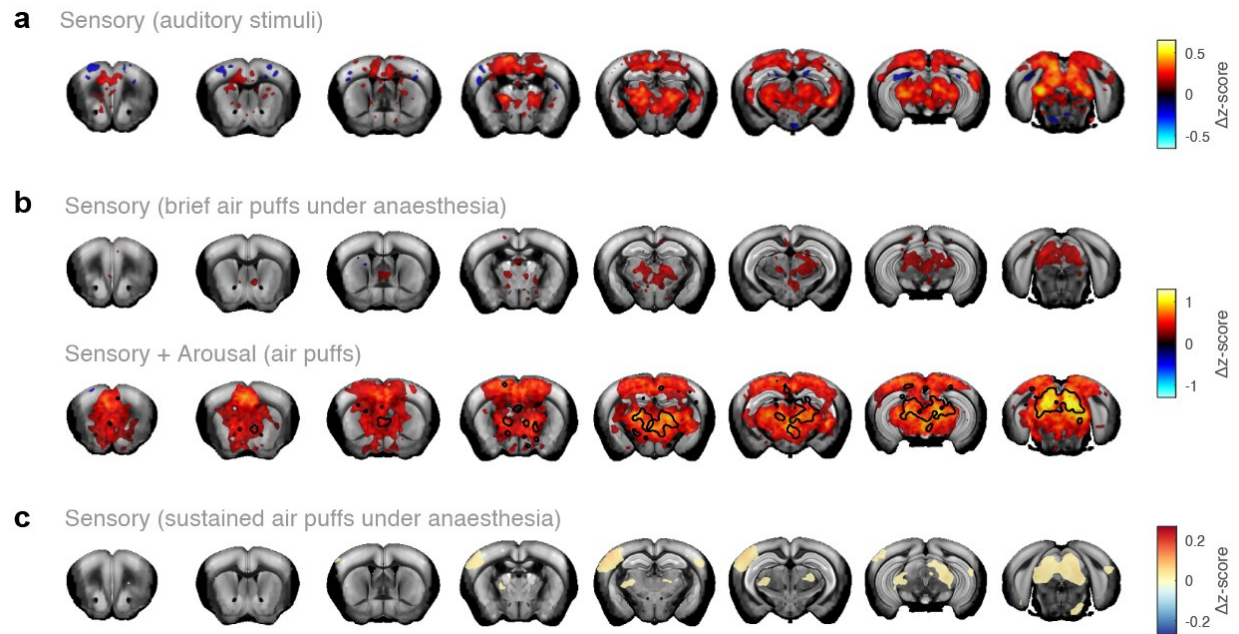
Supp. Figure 4. Fiber photometry signal peaks upon spontaneous and evoked arousal.

a. Diagram of the viral injection and fiber insertion for fiber photometry, and example confocal microscopy images showing GCaMP expressions in anterior cingulate cortex. **b.** Average Ca^{2+} trace in anterior cingulate cortex upon spontaneous pupil events (*left*) and in response to air puffs (*right*), versus average Ca^{2+} trace around control (random) timepoints. ACA: anterior cingulate area.



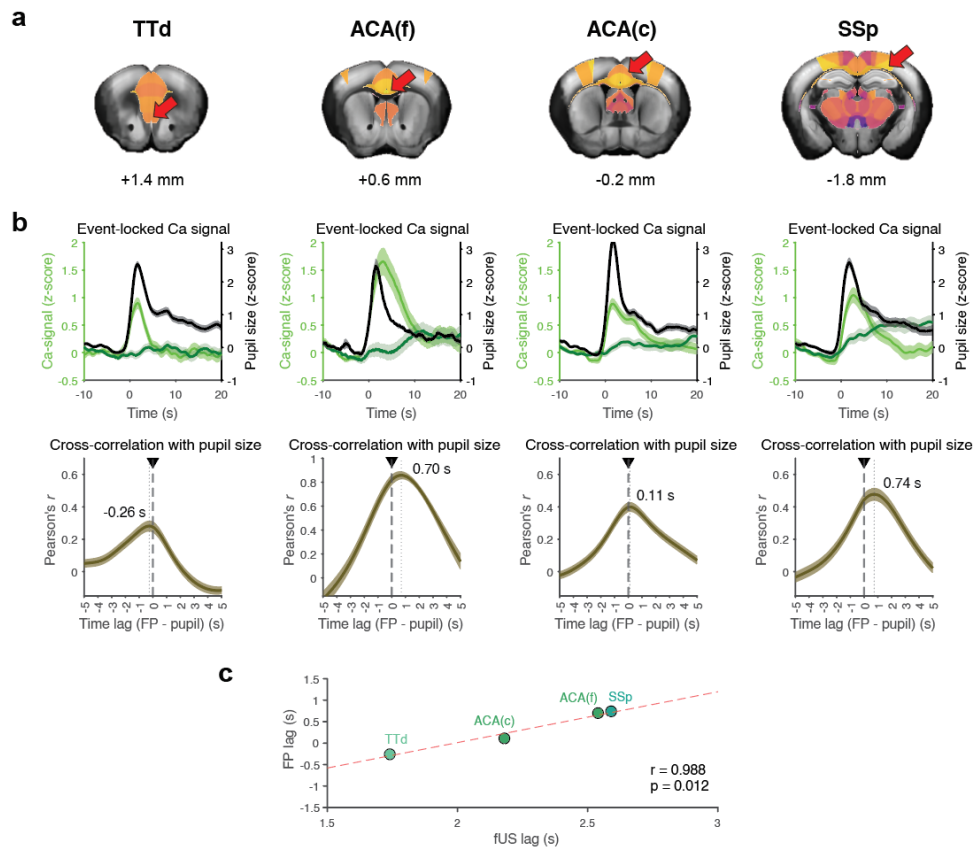
Supp. Fig. 5. Replicability of the arousal responses across mice.

a. Spatial correlation between each frame of the spontaneous (*left*) and evoked (*right*) arousal responses of each mouse. The checkboard pattern suggests that the peak response is consistent across mice. **b.** Spatial correlation between the peak amplitude maps for spontaneous (*left*) and evoked (*right*) arousal responses across mice. **c.** Specificity index of spontaneous and evoked arousal across mice, defined as (correlation with correct template) – (correlation with incorrect template), where the correct template is the average map of the arousal response and the incorrect template is the average map of the pre-arousal baseline. ICC: inter-class correlation.



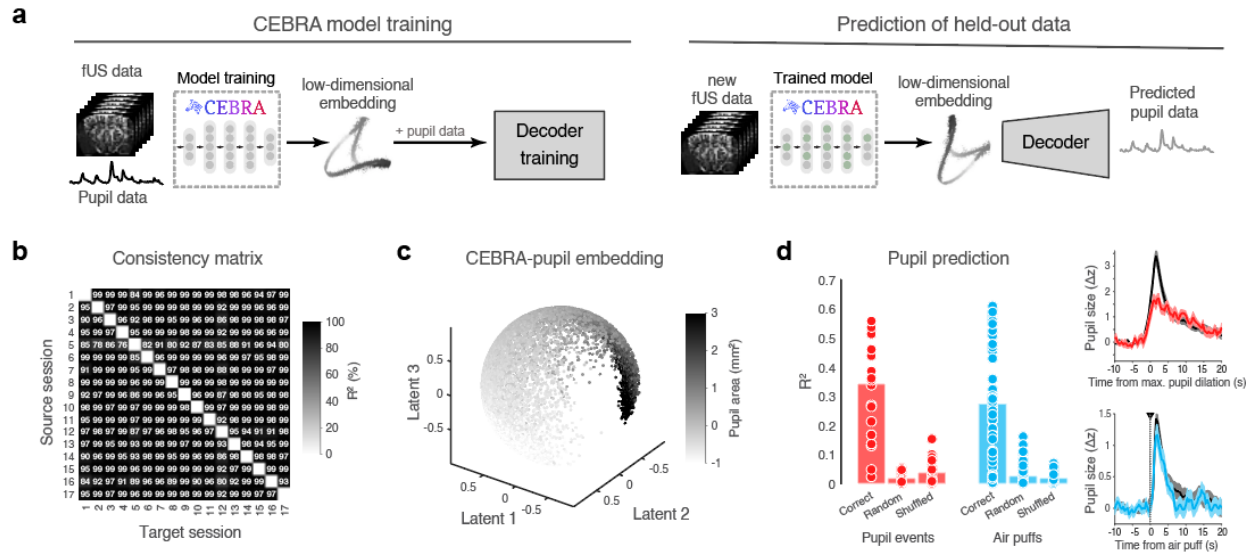
Supp. Figure 6. Evoked arousal response is specific for awake stimulation.

a Average brain-wide fUS response amplitude to white noise, an arousing auditory stimuli (399 stimuli, 7 mice). **b.** Top: average brain-wide fUS response amplitude for brief air puffs under anaesthesia (560 puffs, 7 mice). Bottom: average brain-wide fUS response amplitude for brief air puffs during wakefulness (419 puffs, 7 mice), with the contour of regions still significant under anaesthesia overlaid. **c.** correlation map for sustained air puffs under anaesthesia (28 sessions, 7 mice).



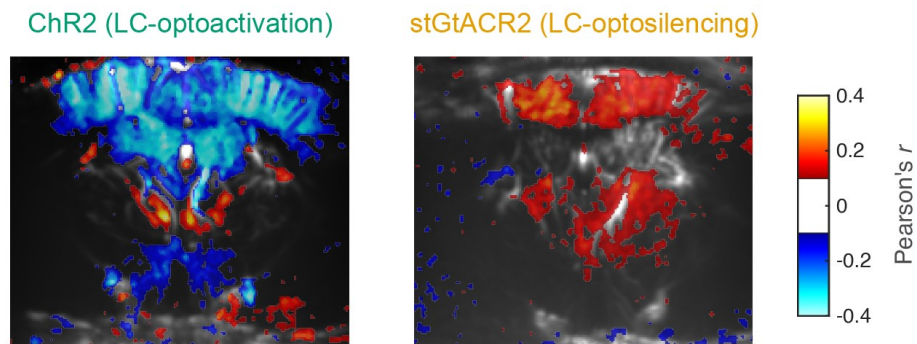
Supp. Figure 7. Fiber photometry signal keeps the same temporal relationship to pupil size as fUS signal.

a. Coronal sections showing the selected regions and their average order of activation as in **Fig. 3**. **b.** Top: average Ca^{2+} traces upon spontaneous pupil events. Bottom: average cross-correlation between Ca^{2+} traces and pupil traces during spontaneous events, used to calculate the delay between both traces. **c.** Scatterplot comparing the fUS and FP average temporal dynamics. TTd: dorsal taenia tecta; ACA: anterior cingulate area (f: frontal, c: caudal); SSP: primary somatosensory cortex.



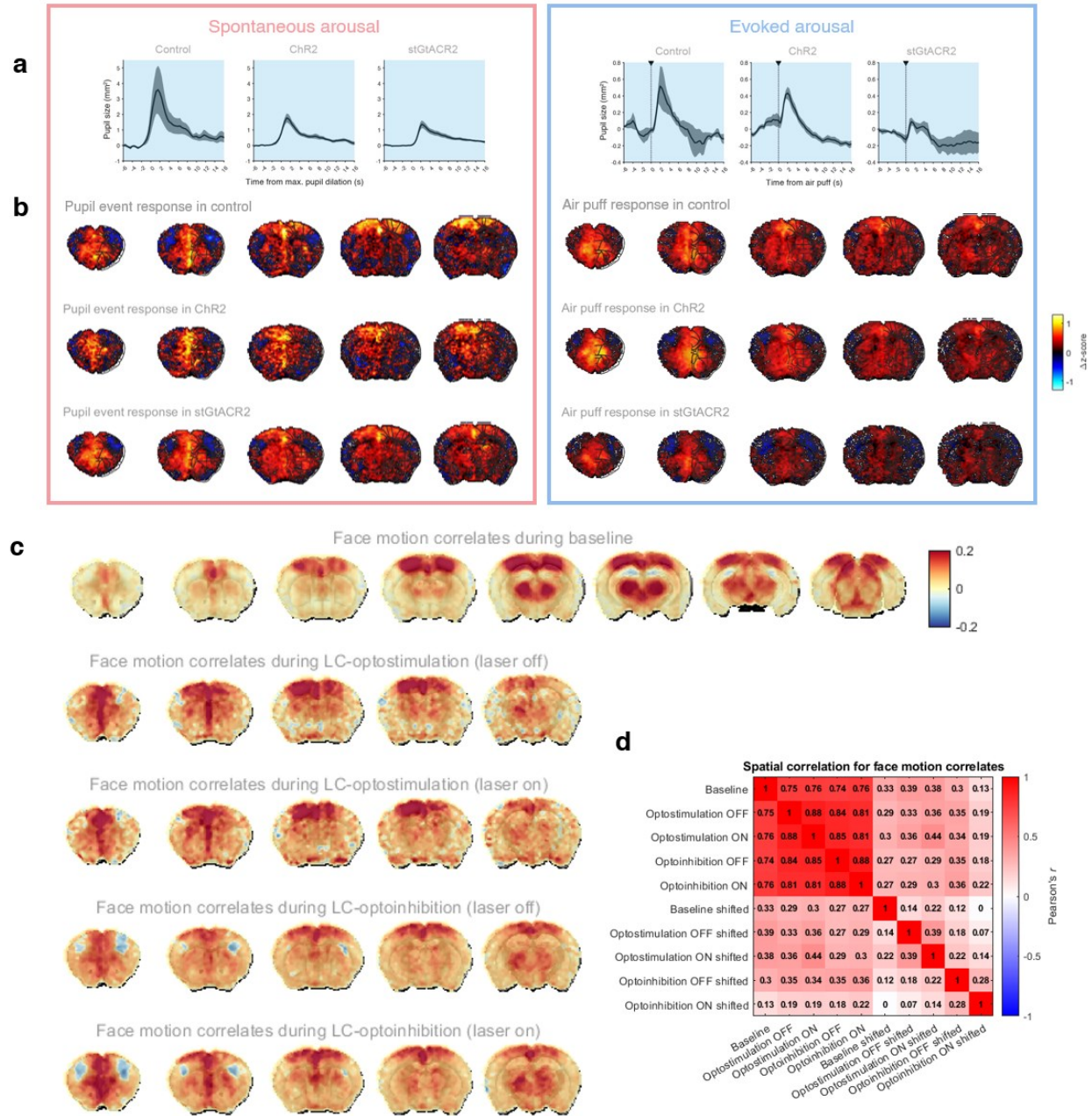
Supp. Figure 8. CEBRA embedding trained on spontaneous fUS signal generalizes to evoked arousal.

a. Schematic of the CEBRA approach. Parcellated fUS data and concurrent pupil size from concatenated baseline (stimulus-free) recordings ($n = 14$ sessions, $N = 7$ mice) were used to train CEBRA and generate low-dimensional representations of the data structure (latent embeddings), which in turn were used to train a kNN decoder. The trained model was used to project new recordings from both stimulus-free ($n = 4$ sessions, $N = 4$ mice) and air puffs ($n = 21$ sessions, $N = 7$ mice) conditions into the embedding, and the trained decoder was used to predict their associated pupil trace. **b.** Consistency matrix showing R^2 values after fitting a linear model between embeddings of independent session pairs. **c.** Latent embedding from CEBRA, plotted using 3 latent dimensions, where each dot represents one timepoint, color-coded by associated pupil size. **d.** Left: barplots representing the average R^2 of the pupil prediction generated by different CEBRA models: trained with correct pupil traces, trained with randomly-permuted pupil traces, and trained with shuffled-across-sessions pupil traces. Right: average pupil trace predicted from the “correct” model for both conditions.



Supp. Figure 9. LC optogenetic stimulation may induce spatially heterogeneous responses in caudal regions.

Example 2D-fUS coronal slices of optostimulation correlates at the caudal end of the imaging field-of-view for the optogenetic cohorts (thresholded for $r > 0.1$), suggesting differential effects of optostimulation in the thalamus.



Supp. Figure 10. Sustained opto-manipulations preserves arousal responses.

a. Average time-locked pupil size during spontaneous (*left*) and evoked (*right*) arousal transitions. **b.** Normalized (z -scored) average brain-wide fUS response amplitude for spontaneous pupil events (*left*) and air puffs (*right*) during concurrent opto-manipulation for all three optomanipulation mice cohorts. **c.** Brain-wide maximum correlation maps of face motion with fUS signal for different mice cohorts. **d.** Matrix of spatial similarity (spatial Pearson's correlation coefficient) between the correlation maps for each mice cohort, including control maps where the face motion regressor has been shifted to eliminate the temporal alignment with fUS signal.

Supplementary table 1: list of common arousal regions as per Allen Brain Atlas demarcation

Primary somatosensory area, lower limb	Primary somatosensory area, trunk	Primary somatosensory area, upper limb
Anterior cingulate area, dorsal part	Anterior cingulate area, ventral part	Anterior visual area
Anteromedial visual area	Primary visual area, anterior lateral	Primary visual area, anterior medial
Primary visual area, posterior medial	Posteromedial visual area	Rostrolateral visual area
Prelimbic area	Infralimbic area	Restrosplenial area, lateral agranular part
Retrosplenial area, dorsal part	Retrosplenial area, ventral part	Taenia tecta, dorsal part
Dorsal peduncular area	CA2 subfield, dorsal part	Induseum griseum
Postsubiculum	Area prostriata	Lateral septal nucleus, rostral (rostroventral) part
Septofimbrial nucleus	Triangular nucleus of septum	Anterodorsal nucleus
Anteromedial nucleus, dorsal part	Anteromedial nucleus, ventral part	Anteroventral nucleus of thalamus
Interanterodorsal nucleus of the thalamus	Intergeniculate leaflet of the lateral geniculate complex	Ventral part of the lateral geniculate complex
Intermediate geniculate nucleus	Subgeniculate nucleus	Central lateral nucleus of the thalamus
Central medial nucleus of the thalamus	Paracentral nucleus	Posterior intralaminar thalamic nucleus
Rhomboid nucleus	Ethmoid nucleus of the thalamus	Posterior complex of the thalamus
Lateral posterior nucleus of the thalamus	Suprageniculate nucleus	Posterior limiting nucleus of the thalamus
Intermediodorsal nucleus of the thalamus	Mediodorsal nucleus of thalamus	Perireunensis nucleus
Submedial nucleus of the thalamus	Parataenial nucleus	Dorsal part of the lateral geniculate complex, core
Dorsal part of the lateral geniculate complex, ipsilateral zone	Medial geniculate complex, medial part	Medial geniculate complex, ventral part
Peripeduncular nucleus	Subparafascicular nucleus, parvicellular part	Posterior triangular thalamic nucleus
Ventral anterior-lateral complex of the thalamus	Ventral medial nucleus of the thalamus	Ventral posterolateral nucleus of the thalamus
Ventral posteromedial nucleus of the thalamus	Lateral habenula	Medial habenula
Zona incerta	Parasubthalamic nucleus	Medial mammillary nucleus, lateral part
Medial mammillary nucleus, median part	Supramammillary nucleus	Posterior hypothalamic nucleus
Central linear nucleus raphe	Interfascicular nucleus raphe	Interpeduncular nucleus, rostral
Interpeduncular nucleus, rostromedial	Rostral linear nucleus raphe	Pedunculopontine nucleus
Substantia nigra, compact part	Anterior tegmental nucleus	Dorsal terminal nucleus of the accessory optic tract
Edinger-Westphal nucleus	Medial accessory oculomotor nucleus	Medial terminal nucleus of the accessory optic tract
Midbrain reticular nucleus, anterior lateral	Midbrain reticular nucleus, anterior medial	Midbrain reticular nucleus, posterior lateral
Midbrain reticular nucleus, posterior medial	Paranigral nucleus	Periaqueductal gray, anterior part
Periaqueductal gray, medial dorsal	Periaqueductal gray, medial lateral	Periaqueductal gray, medial ventral

Periaqueductal gray, posterior dorsal	Periaqueductal gray, posterior lateral	Precommissural nucleus
Nucleus of Darkschewitsch	Interstitial nucleus of Cajal	Supraoculomotor periaqueductal gray
Anterior pretectal nucleus	Nucleus of the posterior commissure	Retroparafascicular nucleus
Red nucleus	Substantia nigra, reticular part	Superior colliculus, deep layers, posterior
Superior colliculus, intermediate layers, anterior lateral	Superior colliculus, intermediate layers, anterior medial	Superior colliculus, intermediate layers, posterior lateral
Superior colliculus, superficial layers, anterior lateral	Superior colliculus, superficial layers, anterior medial	Superior colliculus, superficial layers, posterior lateral
Ventral tegmental area	Inferior colliculus, external nucleus	Nucleus sagulum
Parabigeminal nucleus	Pontine reticular nucleus	